Precipitation features of the Maritime Continent in parameterized and explicit convection models

D. Argüeso*, R. Romero and V. Homar

Meteorology Group, Physics Department, University of the Balearic Islands, Palma, Spain

To be submitted to: *Journal of Climate*

*Corresponding author:
Daniel Argüeso
Edif. Antoni Maria Alcover i Sureda
Cra de Valldemossa km 7.5
University of the Balearic Islands
07122 Palma, Baleares, Spain
Email: d.argueso@uib.es

Early Online Release: This preliminary version has been accepted for publication in *Journal of Climate*, may be fully cited, and has been assigned DOI 10.1175/JCLI-D-19-0416.1. The final typeset copyedited article will replace the EOR at the above DOI when it is published.

Abstract

The Maritime Continent is the largest archipelago in the world and a region of intense convective activity that influences the Earth's general circulation. The region features one of the warmest oceans, very complex topography, dense vegetation and an intricate configuration of islands, which together result very specific precipitation characteristics, such as a marked diurnal cycle. Atmospheric models poorly resolve deep convection processes that generate rainfall in the archipelago and show fundamental errors in simulating precipitation. Spatial resolution and the use of convective schemes required to represent sub-grid convective circulations have been pointed out as culprits of these errors. However, models running at the kilometre scale explicitly resolve most convective systems and thus are expected to contribute to solve the challenge of accurately simulating rainfall in the Maritime Continent.

Here we investigate the differences in simulated precipitation characteristics for different representations of convection, including parameterized and explicit, and at various spatial resolutions. We also explore the vertical structure of the atmosphere in search of physical mechanisms that explain the main differences identified in the rainfall fields across model experiments. Our results indicate that both increased resolution and representing convection explicitly are required to produce a more realistic simulation of precipitation features, such as a correct diurnal cycle both over land and ocean. We found that the structures of deep and shallow clouds are the main differences across experiments and thus they are responsible for differences in the timing and spatial distribution of rainfall patterns in the various convection representation experiments.

Keywords

Convection-permitting models, Maritime Continent, Diurnal cycle, Tropical convection.

Accepted for publication in *Journal of Climate*. DOI 10.1175/JCLI-D-19-0416.1.

1 Introduction

The Maritime Continent (MC, Fig. 1) is an archipelago formed by thousands of islands between the Pacific and the Indian Oceans and spanning 15°S to 15°N. It features complex and steep topography, one of the warmest oceans in the world, densely vegetated land and very intense and frequent convective activity. These elements combined generate specific precipitation characteristics that are highly challenging in terms of atmospheric modelling, of which the most prominent is probably the diurnal cycle. In addition, the MC is a major convective area where strong interactions across scales take place. For example, the presence of the archipelago directly affects and modulates the Madden-Julian Oscillation (Peatman et al. 2013; Birch et al. 2016; Vincent and Lane 2018; Tan et al. 2018), and deep convection in the region is linked to El Niño-Southern Oscillation through the ascending branch of the Walker Circulation (Hendon 2003; Qian et al. 2010). Therefore, convective processes in the region have implications both locally and globally (Neale and Slingo 2003; Yamanaka et al. 2018). A sign of its importance is the international initiative Years of the Maritime Continent (YMC, Phase 1 2017-2020) that joins efforts from researchers and institutions across the world, which overarching goal is "observing the weather-climate system of the Earth's largest archipelago to improve understanding and prediction of its local variability and global impact". From a modelling perspective, a better understanding of the mechanisms driving convection in the MC and improved realism of simulated rainfall in the region is a crucial step towards the overarching goal of the YMC, which will ultimately benefit mesoscale and global climate models alike.

Global climate models typically have spatial resolutions that are unable to represent the complex topography and coastline of the MC. Therefore, they have been largely insensitive to the presence of the islands in the region and have generally produced a dry bias (Neale and Slingo

Accepted for publication in *Journal of Climate*. DOI 10.1175/JCLI-D-19-0416.1.

2003; Schiemann et al. 2013). Although global climate models have undergone substantial improvements in the last decade and are now able to respond better to the presence of the MC archipelago, they still have issues in representing precipitation features such as the amplitude and phase of the diurnal cycle (Baranowski et al. 2019), particularly over land, where model resolution is a limiting factor. However, mesoscale models that typically run at higher resolutions also struggle to reproduce the precipitation regimes in the MC, especially the diurnal cycle (Love et al. 2011; Gianotti et al. 2012) and the land/sea contrasts (Birch et al. 2016; Im and Elthair 2018; Vincent and Lane 2017). Some of the deficiencies are consistent across model resolutions in the mesoscale range and dynamic formulations (i.e. physical parameterizations, dynamical core). For example, simulated precipitation usually peaks too early in the day compared to observations, especially at lower resolutions, and regional models tend to produce too much precipitation over land and too little over the ocean (Gianotti et al. 2012; Kwan et al. 2013; Birch et al. 2016; Hassim et al. 2016; Vincent and Lane 2017; Im and Elthair 2018).

Previous studies (Love et al. 2011; Birch et al. 2015; Bhatt et al. 2016; Baranowski et al. 2019) suggest coarse spatial resolution and the convection schemes may be responsible for the model errors. In continental regions, the positive impact of explicitly resolving convection on the rainfall diurnal cycle timing has already been identified (Grabowski et al. 2006; Hohenegger et al. 2008), and Wagner et al. (2018) came to the conclusion that while resolution is crucial over the mountains, the way convection is represented proves key elsewhere. However, in the MC the presence of the land-sea contrasts adds to the orographic complexity and creates a very specific scenario where sea breeze interacts with orographic lifting to configure rainfall patterns. In this context, Birch et al. (2015) propose that convection is triggered too early in the day by convective schemes, which partly suppress the sea breeze circulation and reduces afternoon rainfall generated by the sea breeze

Accepted for publication in *Journal of Climate*. DOI 10.1175/JCLI-D-19-0416.1.

convergence. As such, the combined effect of very high-resolution and explicit deep convection used in the so-called convection-permitting or convection-resolving models may contribute to alleviate many of the issues of simulated precipitation in the region.

Convection-permitting models are drawing much of the attention of the regional climate modelling community because they constitute a step change with respect to previous resolution increases since they no longer rely on parameterized convection. First results are very promising as convection-permitting models better capture critical precipitation features, such as the diurnal cycle and the spatial patterns (Prein et al. 2015). This especially applies to regions where deep convection is a dominant process (e.g. tropics) and with high spatial heterogeneity (e.g. mountainous areas), both features of the MC. Therefore, one may expect that the potential of convection-permitting models be realized in this part of the globe, where models often miss many of the precipitation characteristics that define local regimes.

The aim of this study is to quantify the impact of increasing resolution and explicitly resolving convection on simulated tropical rainfall of the MC. We identify key precipitation features of the region mostly influenced by these two modelling aspects and put forward physical mechanisms that explain differences between modelling approaches. As such, we understand the term "realism" used throughout the text as rainfall characteristics (i.e., when, where and how it rains) that indicate the model is able to produce precipitating systems and associated circulations that better resemble the observations.

Accepted for publication in *Journal of Climate*. DOI 10.1175/JCLI-D-19-0416.1.

2 Data and experiments

2.1 Model description and experimental design

We use the Weather Research and Forecasting (WRF) modelling system version 3.9.1 to investigate the influence of spatial resolution and convective scheme on the realism of simulated precipitation in the MC (Figure 1).

The model was forced with the latest-generation reanalysis ERA-5 (C3S, 2017), which operates at a spatial resolution of circa 0.3° by 0.3°. This high-resolution forcing data allowed us to design a novel approach to quantify the role of the model spatial resolution by running WRF at multiple resolutions over a single domain in separate experiments (no nesting), all directly driven by ERA5 at their boundaries. This results in a comparable set of simulations at resolutions of 32, 16, 8, 4 and 2 km that run independently from each other and are identical in all other configuration parameters. The approach contrasts with the vast majority of similar previous studies (Holloway et al. 2012; Argüeso et al. 2016; Vincent and Lane 2017; Wagner et al. 2018), which due to computational constrains and boundary data resolution relied on multiple-domain nesting to run at very high resolution, thus necessarily limiting finer resolution runs by deficiencies in the coarser ones. All simulations used a five-grid-point buffer zone that were excluded from the analysis. In addition, when comparing runs at different resolutions, the area covered by the coarsest-resolution buffer zone was removed from all experiments. Thus, in the 2-km runs, this means that the outer 80 grid points in each direction were not considered. This ensure a like-to-like comparison across resolutions.

The model parameterization suite was configured based on a combination of information from previous studies on the region (Argüeso et al. 2016; Li et al. 2016; Vincent and Lane 2016; 2017) and schemes that have been thoroughly used and tested. Sub-grid convective processes were

Accepted for publication in *Journal of Climate*. DOI 10.1175/JCLI-D-19-0416.1.

139 modelled with the Betts-Miller-Janjic (BMJ) scheme, which is a profile-adjustment
140 parameterization of both deep and shallow convection designed for tropical convection (Betts
141 1986; Betts and Miller 1986; Janjic 1994). Runs with the BMJ scheme are labelled with DP (Deep
142 convection Parameterized). In order to determine the influence of the convective scheme, two
143 additional experiments were completed at all resolutions: a first one assuming deep convection is
144 resolved (SH), thus including only a shallow convection scheme (Hong and Jang 2018); and a
145 second one assuming all convection is explicitly resolved by the model (EX). Besides the fully-
146 explicit run, we also analyse the impact of a shallow convection scheme because we can only
147 expect large deep convective cells be represented at scales near 4 km, thus convective circulation
148 that occurs in the lower troposphere should be parameterized. This circulation generates low-level
149 clouds that hardly produce any rainfall but do indeed have an influence on the vertical mixing and
150 directly interact with deep convection mechanisms either cooperating or competing (Lee et al.
151 2003, Khairoutdinov and Randall 2006, Schlemmer and Hohenegger 2014, Pilon et al. 2016).
152 Although the two assumptions above regarding shallow and deep convection are clearly not
153 true for all resolutions and may only hold at 4- and 2-km resolutions, we explore these
154 configurations at all resolutions to show the separate effect of resolution and parameterized
155 convection on the realism of precipitation in the region. This helps to establish whether any
156 potential improvement is due to both factors acting together or any of them independently.
157 A summary with additional details on the model parameterizations chosen is provided Table 1.
158 Because of the importance of microphysics for precipitating processes, it is worth noting we used
159 the WRF Single-Moment 6-class scheme (WSM6, Hong and Lim, 2006), which includes water
160 vapor, cloud water, cloud ice, graupel, rain and snow. We also run a few preliminary tests using a
161 more complex microphysics scheme (Thompson et al. 2008), two mass-flux convective schemes

Accepted for publication in *Journal of Climate*. DOI 10.1175/JCLI-D-19-0416.1.

(Multi-Scale Kain-Fritsch, new Tiedke) and the recommended tropical physics suite (NCAR, 2017). None provided better precipitation estimates than the chosen configuration over the MC (not shown).

All experiments span one austral summer (1st November 2015 to 29th February 2016) and include a 10-day spin-up period (22nd- 31st October 2015) that is discarded from the analyses. A longer spin-up period (60 days) was also tested to determine its influence on the precipitation outputs. Extending the spin-up considerably increased the computational cost while it did not have any substantial impact on the atmospheric variables and thus on the model performance in terms of precipitation. Although longer periods are needed to draw conclusions at climatological scales, the computational requirements of these simulations currently preclude longer experiments. We conducted runs for two additional austral summers (2013/14 and 2014/2015) for some of the resolutions to ensure the results are not dependent on the year chosen (not shown). We also performed an additional two-month run at 4-km with no convective scheme (i.e. EX) and expanding the domain 100 grid points to test the impact of the resolution jump at the boundaries. We only found minor differences between the results (not shown), which did not warrant the computational costs associated with a larger domain. All model outputs were saved at hourly frequency to examine the sub-daily features of rainfall and convective processes.

2.2 Observational products

A collection of satellite-derived rainfall products is used as observational reference, hereafter referred to as observations for brevity. Despite the fact that such products are known to have non-negligible deficiencies (Ebert et al. 2007; Vernimmen et al. 2012; Matthews et al. 2013; Bharti et al. 2015; Tan et al. 2015; Skok et al. 2016; Vincent and Lane 2016; Rauniyar et al. 2017; Rahmawati and Lubczynski 2017), particularly near the coast and in mountainous regions (Hirpa

Accepted for publication in *Journal of Climate*. DOI 10.1175/JCLI-D-19-0416.1.

et al. 2010; Vernimmen et al. 2012; Matthews et al. 2013; Chen et al. 2013), it is the closest reference to reality in a region characterized by very sparse in-situ data. To this purpose, we have chosen four different datasets.

The multi-satellite product generated with the Climate Prediction Center (U.S.) morphing technique (Joyce et al. 2004) is a global precipitation analysis available at approximately 8-km spatial resolution (0.0727°) and 30-min temporal resolution, aggregated into hourly frequency here. Precipitation estimates are derived from passive microwave scans and infrared geostationary data. It comes in two versions, the original satellite estimates (CMORPH_RAW) and a bias-corrected product using rain gauges (CMORPH_CRT).

The Tropical Rainfall Measuring Mission (TRMM 3B42v7 2011, Huffman et al. 2007) multi-satellite precipitation analysis provides quasi-global rainfall estimates on a 0.25° (~ 27.5 km) resolution grid and a 3-hourly frequency. This dataset is widely used in studies of tropical precipitation and is currently a standard reference. TRMM is also generated using both passive microwave and infrared information. Satellite-derived information is complemented with two monthly rain gauge analyses developed by the Global Precipitation Climatological Center and the Climate Prediction Center (U.S.).

The Global Precipitation Measurement (GPM) created with the Integrated Multi-satellite Retrievals for GPM (GPM_3IMERGHH v05, Huffmann 2017) is a global precipitation dataset at 0.1° (~ 11 km) spatial resolution and 30-min temporal resolution that builds upon TRMM. It generates rainfall estimates from intercalibrated space-borne radio wave instruments (dual frequency precipitation radar), active and passive microwave measurements and precipitation gauge analyses.

Accepted for publication in *Journal of Climate*. DOI 10.1175/JCLI-D-19-0416.1.

This ensemble of precipitation products provides a range of rainfall values for each time and location, and thus serves as an estimate of the observational uncertainty associated with satellite-derived information. As such, it is a way to incorporate this uncertainty in the model performance evaluation. For comparison purposes, all datasets were interpolated to the highest resolution grid (2 km) using a nearest-neighbour approach. This ensures that the interpolated field conserves spatiotemporal variability and areal-averaged values compared with the original field (Di Luca et al. 2016).

3 Results

In this section, we first analyse the domain-averaged model outputs to provide an overall assessment of the model performance. Then we examine the spatial detail of the simulated precipitation for the 4-km experiments. Finally, we investigate differences in the vertical structure of the atmosphere between the various 4-km runs with the purpose of putting forward a physical interpretation of the impacts from the convection representation.

3.1 Precipitation

The domain-average mean precipitation is a first-order measure of the model water balance physical realism. Figure 2a shows the domain-averaged precipitation mean from the various observations and all model simulations for the 2015-2016 austral summer. According to these results, the model is overall well-calibrated and total precipitation amounts generated by the model remain within 35% of the observations average for the entire domain in the worst case (32-km resolution). This agreement with observations improves steadily as we move to higher resolutions in the DP experiments. Overall, the model produces too much precipitation with the deep convection scheme (DP), but the biases are corrected with increased resolution to less than 10% at

Accepted for publication in *Journal of Climate*. DOI 10.1175/JCLI-D-19-0416.1.

2-km grid-space. The use of shallow convection scheme tends to produce too little precipitation overall and resolution has a positive impact only for the coarsest cases (from 32 km to 8 km). The fully-explicit convection (EX) runs produce accurate estimates of domain-wide precipitation at all resolutions (within 10% of the observations average for the 32-km run, and within 5% for the rest). In fact, EX provides the best domain-averaged precipitation values of the three configurations at all resolutions, despite most convective circulations not being explicitly represented at resolutions between 8 and 32 km. It is interesting to note that experiments with explicit deep convection (SH and EX) show little to no improvement when increasing resolution beyond 8 km. Indeed, most EX runs produce total precipitation amounts within the observational range (grey bars, Fig. 2).

However, this apparent agreement is consequence of a compensation of errors over land and ocean (land fraction is between 18.4% and 18.8% in all simulations), where the mechanisms producing rainfall may be quite different. Averaged across the domain, the model generates too much precipitation over land (Fig. 2b) and too little over the ocean (Fig. 2c), except for parameterized deep convection (DP) that tends to overestimate rainfall over water too. This is in agreement with previous studies using either the same model (Hassim et al. 2016; Vincent and Lane 2017) or different ones (Love et al. 2011; Birch et al. 2016; Im and Elthair 2018). Increasing resolution has a positive effect on DP experiments by reducing the wet bias both over land and water, but the other two experiments (SH and EX) seem to worsen at higher resolution over land and show only some improvement over the ocean. For example, EX runs deviate from the observations average over land between 44% (32 km) and 75% (2 km) whereas SH does so by 44% (32 km) and 71% (2 km). Over the ocean, explicit representation of convection reduces the amount of precipitation to values below observations, especially when parameterizing shallow convection (SH), for which the bias varies between -50% (32 km) and -39% (8km). These results

Accepted for publication in *Journal of Climate*. DOI 10.1175/JCLI-D-19-0416.1.

highlight the role of convection representation over the influence of resolution, particularly over the ocean.

According to Figure 2, it may be argued that increasing resolution beyond 8 km only brings some benefit with parameterized deep convection, while experiments with explicit deep convection perform best at low or intermediate resolution (8 km). This may seem contradictory with most of the literature that identifies the range between 4 and 10 km as the convective grey zone where explicit and parameterized convection may compete with each other, degrading the results (Prein et al. 2015). However, the domain-averaged total precipitation, even if split into land- and ocean-only grid cells, only provides first-approach information on the model rainfall realism. Thus, we also examine the precipitation diurnal cycle, which requires the model to better represent local forcing and local circulation in order to capture it.

In the MC rainfall has a very distinct diurnal cycle, especially over the islands. Differential solar radiative heating between different surface types cause local pressure gradients that result in land-sea breeze circulations, which in combination with orographic lifting and downslope mountain winds at night, constitute key precipitating mechanisms in the region (Qian 2008; Birch et al. 2015). Although subject to spatial variations due to propagation of precipitating systems, rainfall generally peaks between late afternoon and early evening over land, while over water, precipitation reaches it maximum in the early morning, albeit with a much smaller diurnal cycle amplitude than over land.

Figure 3 depicts the mean diurnal cycle of precipitation over land and ocean grid points averaged over the entire domain. Over the islands, all experiments overestimate the amplitude and the mean of the diurnal cycle (i.e., vertical shift of the cycle), consistent with Figure 2b. Bhatt et al. (2016) obtained similar results for various convective parameterization schemes with the same

Accepted for publication in *Journal of Climate*. DOI 10.1175/JCLI-D-19-0416.1.

model, but completely different physics configurations. They suggest that the misrepresentation of mechanisms related to boundary layer transfer and convective lifting-condensation-precipitation in parameterization schemes may be the cause of the exaggerated amplitude over land and had expectations that convection-permitting experiments may contribute to address this issue. None of the experiments proposed here, including those at 2-km spatial resolution and fully-explicit convection, alleviate the problem with the amplitude of the diurnal cycle. Quite the opposite, increasing resolution tends to amplify the diurnal cycle over land. However, at 2-km spatial resolution, there are crucial processes in the development of moist convection that remain unresolved, such as cloud turbulence and the interaction between the cloud and the environment (Bryan et al 2003), which may cause too strong convection and therefore may explain these issues. The transition from convective to stratiform rain has also been identified as one of the weaknesses in convection permitting models operating at spatial resolutions in the range 1-4 km (Caine et al. 2013, Vincent and Lane 2018).

Despite the fact that the amplitude remains too strong in all experiments, the phase of the diurnal cycle is significantly improved by the combination of finer resolution and the absence of a deep convection scheme. Parameterized deep convection experiments produce precipitation too early compared to the observational range. In the observations, precipitation initiates at 10LST (Local Solar Time) and peaks at 17-18LST, while these two events occur a few hours ahead in the DP cycle (07LST and 15-16LST). By just increasing resolution, DP experiments are only able to improve the night-time and early morning values thank to a more accurate decay in evening rainfall rates, but the errors in the phase and amplitude of the diurnal cycle are worsened in most cases.

Using explicit deep convection (SH and EX) corrects the phase of the diurnal cycle at high resolutions. In fact, the model captures the observed phase when deep convection is not

Accepted for publication in *Journal of Climate*. DOI 10.1175/JCLI-D-19-0416.1.

298 parameterized and resolution is 8 km or finer. On the other hand, these experiments render a
299 delayed diurnal cycle with respect to observations when running at 32 and 16 km, but the amplitude
300 compares better with satellite products than other resolutions. As we move to higher resolutions,
301 the model amplitude increases and the phase advances, which means better agreement with
302 observations in the timing, but also overestimation of the precipitation amounts, especially at the
303 time of maximum rainfall. The average timing of maximum precipitation across satellite products
304 is slightly after 17LST, thus the 2-km resolution seems the best match for the diurnal cycle phase
305 in terms of the rainfall peak. The time of the cycle minimum averaged across observations is
306 located between 09 and 10LST, which makes both the 4-km and 2-km the closest to observations.
307 The response of the phase to increasing resolution is similar for both explicit convection and
308 shallow convection runs (i.e. advancing the peak from 22LST at 32 km to 17LST at 2 km), but SH
309 simulations tend to produce less rain and the amplitude is thus closer to observations. The reason
310 that explains the delay in the diurnal cycle with respect to DP may be different in both experiments.
311 The EX run may need more Convective Available Potential Energy (CAPE) to trigger convection
312 than the DP case, while the shallow convection scheme removes CAPE without producing any
313 rainfall.

314 The response to both resolution and convective representation is more coherent over the ocean
315 (Fig. 3b), where simulations with different convective representation are clearly clustered in three
316 groups. The amplitude of the cycle and the mean precipitation compares better with observations
317 in the parameterized deep convection (DP) experiment than the other two. DP is followed by EX
318 and SH runs in this order, and both underestimate rainfall. This is consistent with results obtained
319 in Figure 2c. However, in terms of the diurnal cycle phase any of the experiments seems to
320 outperform the others. DP produces an accurate timing of the maximum, but the minimum of

Accepted for publication in *Journal of Climate*. DOI 10.1175/JCLI-D-19-0416.1.

precipitation is slightly early compared with observations. Despite the fact that EX and SH simulate drier conditions than DP and satellite-derived products, there are features of the diurnal cycle shape in the explicit deep convection runs that better match the observations. For example, the timing of the minimum in the evening hours and the following intensification of precipitation is closer to observations in EX and SH. Increasing resolution improves all simulations, by producing less rain in DP and intensifying the amplitude in EX and SH, although resolution plays a role in improving rainfall rates only up to a certain threshold (8 km SH and EX, and 4 km in DP). Simulations are ranked according to their performance in different metrics of the diurnal cycle in Table 2.

Given the limited benefit from the highest resolution runs (2-km) showed so far, and the enormous increase in storage requirements for those experiments, which add to the computational demands, we will focus on the 4-km simulations from now on. In addition to the domain-averaged model performance described above, we examine the spatial distribution of both the precipitation rates and the diurnal cycle to determine whether the model is able to locate rainfall at the right time and place and identify differences across experiments.

Figure 4 shows the spatial distribution of rainfall biases for all 4-km runs with respect to the range of observations. Following Evans et al. (2016) the bias is calculated with respect to the closest observational value and the model estimates are considered equivalent to observations when within the observational range (i.e. bias set to zero). As a result, this approach incorporates the uncertainty in the satellite-derived products. The fully-explicit convection experiment (EX) produces a mean absolute error of 35.1% and slightly outperforms the other two (DP 39.8% and SH 48.5%). Although with different mean absolute errors, this relative performance of the various experiments is consistent across resolutions within the convection-permitting scale range (2 and 4

Accepted for publication in *Journal of Climate*. DOI 10.1175/JCLI-D-19-0416.1.

km), the convective grey zone (8 km) and just above (16 km) (Supplementary Figure S1). However, at coarser resolutions (32 km), the need for a convective parameterization becomes evident, as the DP experiments provide better estimates (51.8% for DP, 53.2% for EX and 64.5% for SH). These results align with the scale separation often used for convective processes into convection-permitting (<4 km) and parameterized convection (>10 km) scales (Prein et al. 2015), although DP and EX mean absolute error values are very close to each other at most resolutions and thus none can be considered superior, especially for summer-long simulations like these.

At coarse resolutions wet biases dominate over the ocean across the domain in DP runs, while the opposite occurs in explicit deep convection runs (Supplementary Figure S1). This is likely due to the fact that the convective scheme readily triggers, which tends to produce deeper clouds and precipitates more easily (see Section 3.2). Increasing resolution makes this contrast diminish between DP and EX, and they seem to converge. However, all experiments using the shallow convection scheme are consistently dry over the ocean, where SH runs struggle to generate precipitation. For example, to the southwest of Sumatra and Java, SH underestimate rainfall by 80% or more, which means it barely produces any rain.

Figure 4 shows that wet biases obtained over land from all 4-km experiments are mostly concentrated over mountainous regions. Simulations with explicit deep convection (SH and EX) show a better agreement with observations at low-lying areas in large islands such as New Guinea and Sumatra, but exacerbate rainfall amounts at higher elevations. For instance, averaging over grid cells above 1000 m, which are approximately 10% of all land grid cells, the model produces mean absolute errors with respect to the observational range of 188% for DP, 255% for EX and 262% for SH (Supplementary Figure S2). This agrees with previous studies that used different models (Birch et al. 2015; Holloway et al. 2012; Leutwyler et al. 2017), which also produce too

Accepted for publication in *Journal of Climate*. DOI 10.1175/JCLI-D-19-0416.1.

much precipitation over high orography when switching the convective scheme off. Hassim et al. (2016) attributed these errors to the grid space they used (4 km). We already showed that taking resolution beyond 4-km has little impact when considering the entire domain, but focusing on high orography (>1000m) the 2-km resolution contributes to fix the precipitation wet bias (137% for DP, 189% for EX and 211% for SH) as anticipated by Hassim et al. (2016), although the model still deviates considerably from observations. However, it should be noted that satellite-derived rainfall products have been consistently found to have issues over complex topography (Ebert et al. 2007; Matthews et al. 2013; Skok et al. 2016), including New Guinea, where Vincent and Lane (2016) obtained errors comparable to model biases shown here when analyzing precipitation data from gauges and satellite estimates. Multiple reasons have been proposed for these problems, including scattering of the microwave signal by mountains (Huffman et al. 2007), misdetection of warm clouds at the top of the mountains by infrared sensors (Yilmaz et al. 2005) and underestimation of heavy rainfall events from shallow orographic systems by microwave algorithms (Shige et al. 2013), among others. In the MC, satellite-derived products tend to underestimate rainfall at high elevations and overestimate coastal precipitation (Vernimmen et al. 2012; Rauniyar et al. 2017). This indicates that, although the model is clearly prone to significant errors over mountainous regions, simulated precipitation may be closer to actual values than what Figure 4 suggests.

As a fundamental aspect of rainfall in the region, the phase of the diurnal cycle throughout the domain is analyzed. This is done by fitting the diurnal cycle of precipitation at each grid point to the diurnal harmonic following similar studies (Bhatt et al. 2016; Baranowski et al. 2019). Figure 5 shows the phase of the diurnal harmonic, specifically the time of maximum precipitation, for CMOPRH_CRT and all 4-km simulations. Results for all other resolutions is provided in the

Accepted for publication in *Journal of Climate*. DOI 10.1175/JCLI-D-19-0416.1.

supplementary material (Supplementary Figure S3). In the 4-km runs, improvements from explicit deep convection experiments (SH and EX) are evident for this feature of rainfall in the MC, particularly over the largest islands of the domain, such as New Guinea, Borneo and Sumatra. For example, the propagation of convective precipitation systems from coastal areas towards the interior of the islands better agrees with observations in EX and SH simulations. In the DP experiment, peaks at 12-18LST dominate most of the land, while maxima at 18-02LST prevail in the observations and the other two runs. In some islands, observed rainfall peaks earlier in the mountains (e.g. Java, New Guinea, Sumatra) and then propagates downslope (see Section 3.2), a feature well-represented in the model as well. However, in Borneo, rainfall propagates from the coast to the mountains, where it peaks at from 12-13LST in the east coast to 04-05LST in the central mountains. This feature is better captured in EX and SH. The differences in the spatial patterns of the rainfall peak timing is consistent with previous findings (Grabowski et al. 2006; Hohenegger et al. 2008; Argüeso et al. 2016) that showed the positive impact of convection-permitting runs on the timing of the rainfall diurnal cycle over land. Over the ocean, a diurnal cycle is identified in observations with this method (i.e. using a minimum threshold of 0.1 mm hr-1 in the amplitude of the fitted harmonic to identify areas with a defined diurnal cycle) in regions around the islands, such as the Java and Bismark seas. In these areas, precipitation usually peaks between night and early morning (00-06LST) near the coast and propagates to open waters (06-12LST). Although not as spatially coherent, all experiments broadly capture this pattern, with SH producing the peak slightly earlier (e.g. Java Sea).

The impact of resolution in the timing of the rainfall peak over land is more prominent when explicitly resolving deep convection (Supplementary Figure S3). For example, in the EX experiments, the rainfall maximum is delayed at coarser resolutions (00-06LST, 32km) and it

Accepted for publication in *Journal of Climate*. DOI 10.1175/JCLI-D-19-0416.1.

occurs progressively earlier as resolution increases. A similar behavior is obtained for the SH runs. On the other hand, resolution only has a marginal effect on the phase of the diurnal cycle when parameterizing deep convection. These results suggest that the deep convection scheme contributes to producing the diurnal cycle too early, with nearly no improvement with resolution. However, when the convective scheme is not used, resolution plays a key role. This is not necessarily surprising, since convection-permitting resolutions are required to effectively resolve convective systems. Indeed, once the model enters the convective gray zone and begins to reproduce large convective systems (>10 km), increasing resolution has only a limited impact on the phase of the diurnal cycle. This shows that resolution must reach convection-permitting scales and the deep convection scheme be turned off to benefit from an improved diurnal cycle timing, although the gain is limited above a certain threshold (8 km). The 8-km runs may be favored by the fact that the resolution of the CMORPH final product is also 8 km, and therefore higher-resolution runs may pay a penalty because small scale (< 8 km) variability is not represented in the observations.

3.2 Vertical structure of the atmosphere

In this section, we examine aspects of the vertical structure of the atmosphere to reveal possible physical mechanisms that explain the differences in precipitation across convective representations in the model.

Firstly, the stability of the atmospheric column is examined through the maximum CAPE as a precursor of deep convection and the maximum convective inhibition (CIN) as the initial energy needed to reach the level of free convection (Fig. 6). Both were calculated for the parcel with maximum equivalent potential temperature within the lowest 3000 m (Ladwig, 2017). Given the

Accepted for publication in *Journal of Climate*. DOI 10.1175/JCLI-D-19-0416.1.

contrasting response to convective representation at high and low resolution, we performed this analysis for runs at 4- and 32-km grid sizes.

Over land, fully explicit convection (EX) produces substantially larger CAPE values than parameterized convection, both shallow and deep, throughout the day. In the high-resolution runs, differences could reach up to 40% more during the early afternoon (Fig. 6a). This could partly explain why EX tends to produce a stronger diurnal maximum than SH over land because higher CAPE values are linked to more intense deep convection once it is activated and, both EX and SH depend on the same triggering factors to develop deep convection. However, this does not apply when deep convection is represented differently because the generation of rainfall not only depends on the potential intensity of convection but also on whether it is triggered or not. Indeed, examining CAPE also for the 32-km experiments (Fig. S4) shows that higher precipitation peaks cannot be directly attributed to higher CAPE values since deep moist convection must develop in order to transform such instability into precipitation. Factors that help initiate convection (i.e., orographic lifting, sea-breeze, convergence lines, surface heterogeneities, rising thermals, cold pools) are generally fine-scale features and thus mostly unresolved at coarse resolutions. This explains why in spite of EX runs accumulating more CAPE, this does not always reflect on the precipitation diurnal cycle. Although SH experiments depend on triggering factors in a similar way, the shallow convection scheme is more efficient at removing CAPE in the lower levels through parameterized non-precipitating processes, hence it does not accumulate as much CAPE as EX.

On the other hand, the BMJ deep convection scheme does not rely on triggering mechanisms and acts by relaxing an unstable profile towards a stable one, thus incorporates such factors implicitly at the sub-grid scale. Therefore, the fact that DP uses a relaxation scheme that depends

Accepted for publication in *Journal of Climate*. DOI 10.1175/JCLI-D-19-0416.1.

458 on the environmental conditions as opposed to EX and SH, makes it activate deep convection more
459 easily and thus is prone to produce rainfall early in the day.

460 Likewise, in the ocean, both explicit deep convection experiments (EX and SH) simulate values
461 of available convective energy approximately 20% larger than the fully parameterized case at 4-
462 km (Fig. 6b), but they tend to produce significantly less precipitation than DP. Therefore, EX and
463 SH do not trigger convection often enough over the ocean and therefore they are not efficient at
464 transforming this energy into precipitating systems. A plausible reason is that, over the ocean, the
465 model may lack triggering factors compared to land, where the model does have them, yet not
466 completely resolved. For example, one of the triggering mechanisms in the ocean are the Sea
467 Surface Temperature (SST) gradients (Sabin et al. 2012) and in our simulations they are only partly
468 captured because SST is directly obtained from ERA5. In the case of SH, domain-average CIN
469 over the ocean is also slightly larger (~20%) than DP and EX, which could contribute to hinder
470 parcels reaching the LFC (Fig. 6d).

471 We further investigate the vertical structure of the atmosphere through cross-sections of
472 temperature, humidity and clouds across New Guinea from EX and DP. Figure 7 and 8 focus on
473 vertical transects at 11 and 16LST. The entire diurnal evolution is shown in the supplementary
474 material (Supplementary animation 1). Overall, fully-explicit convection generates a warmer and
475 moister atmosphere than the deep convection parameterization in the lowest kilometer, and a
476 cooler and drier atmosphere in the upper levels. Although over the ocean a layer of cooler air is
477 also generated near the surface. A warmer and humid layer near the surface indicates that EX
478 produces shallower vertical transport of heat and moisture, and thus is less efficient at mixing the
479 free troposphere. This structure describes a more unstable atmosphere and therefore larger CAPE
480 values, consistent with Figure 6. However, as mentioned above, the lack of triggering mechanisms

Accepted for publication in *Journal of Climate*. DOI 10.1175/JCLI-D-19-0416.1.

481 over the ocean prevent the fully explicit run to transform that instability into precipitation. That is,
482 as we mentioned above, there is potential for more intense convection in EX, but it is not triggered.
483 Surface evaporation over the ocean is very similar in both experiments thus the moist lower layer
484 is caused by capped mixing in EX rather than higher water vapor input from the water surface. It
485 is likely that the excess of humidity in EX is advected to the island by the dominant winds from
486 the ocean, which are then lifted by topography and sea-breeze circulation to produce more rainfall
487 than in the DP run.

488 The evolution of winds and clouds throughout the day provides an interesting insight on the
489 processes generating rainfall in each case, and point to possible causes of differences in the
490 precipitation diurnal cycle. A feedback between early rainfall and sea-breeze dying out has been
491 proposed as a mechanism that may explain why parameterized convection does not capture the
492 diurnal cycle adequately (Birch et al. 2015). However, our results show that the sea-breeze is
493 synchronized across simulations. In both experiments, it originates at around 10-11LST (Fig. 7c
494 and d, highlighted in red), propagates inland at 13LST and then vanishes at around 18-20LST, as
495 shown by the sea-breeze front in the southwest coast of New Guinea (Supplementary animation
496 1). Therefore, the sea-breeze and convective initiation feedback does not explain differences in the
497 precipitation diurnal cycle according to our model runs. The convective initiation over the
498 mountains and its intensity does not seem to be a cause of the differences either, since its
499 development is very similar in both experiments.

500 The most notable difference introduced by the fully explicit representation of convection is
501 obtained in the cloud structure and the associated rainfall patterns. EX tends to produce a layer of
502 shallow clouds covering large areas of the island that start at 09LST and persists until the night
503 (See Suplementary animation 1), albeit displaced towards inland and lifted upwards. It is

Accepted for publication in *Journal of Climate*. DOI 10.1175/JCLI-D-19-0416.1.

interesting to note that this layer is not associated with almost any precipitation, except at the sea-breeze front (Fig. 8d). DP also produces a layer of shallow clouds, but it is confined and strongly tied to the sea-breeze front, thus covering a much smaller area (Fig. 8c). By contrast, DP produces much deeper clouds that extend over the entire island and start at around 10-11LST (Fig. 7c) and are mature by 16LST (Fig. 8c). These deep clouds seem to be responsible of differences in rainfall between the two runs. Indeed, DP produces much more precipitation between 12LST and 17LST over the large flat areas of New Guinea, while EX precipitation is concentrated in the mountains and barely generates rainfall in that part of the island until the evening (Figs 7-8 and supplementary animation 1). This is key to explain differences in the land-averaged diurnal cycle differences between DP and EX. Our analysis does not allow to determine the origin of deep clouds in DP, but according to differences in the wind patterns between 12 and 18 LST in the upper troposphere (dashed red rectangle in Fig 8c, d), they do not appear to be generated only by propagation from the mountain convective center as in EX, but air lifted throughout the island contributes to their formation too (Fig. 8c). In fact, during the central hours of the day (12-18LST), EX produces wind patterns with subsidence in the upper troposphere, while DP shows a general updraft. These results are not exclusive to New Guinea and are comparable to cross-sections across other islands (not shown).

Similar results were obtained for SH too (Supplementary Figures S5 and S6). The shallow convection run also generates a lower layer that is warmer than DP together with a cooler atmosphere above at 11LST. This is also accompanied by a thin wetter layer in the lower levels and drier conditions above. In the afternoon (16LST), the warm difference with DP extends a few kilometres high (~ 5km) and the wet difference with respect to DP over land intensifies. The difference with DP in the structure of clouds may be divided into deep and shallow clouds. SH

Accepted for publication in *Journal of Climate*. DOI 10.1175/JCLI-D-19-0416.1.

tends to produce shallower clouds over land and less deep clouds than DP. This result is very similar to what we obtained for EX. Differences between EX and SH (Supplementary Figures S7 and S8) shed light on the effect of the shallow cumulus parameterization alone, which mostly affects the lower levels of the troposphere over land (< 3 km). Consistent with the expected behaviour of the shallow cumulus scheme (Stensrud, 2009), shallow convection schemes generate a vertical dipole because it cools and moistens the upper half of the cloud layer and warms and dries the lower half of the cloud layer (with respect to the fully explicit case). Over the ocean, the effect of the shallow cumulus scheme extends to higher levels (up to 6 km), particularly in terms of humidity (Supplementary Figure S7b and S8b). The shallow cumulus further intensifies the mid-troposphere drying we obtained for EX. This is likely the consequence of SH vertically capping convection over the ocean, which leads to smaller precipitation rates.

An individual analysis of cloud water and ice mixing ratios reveals additional details on the contrasting cloud structures in the various runs and the corresponding precipitation diurnal cycles. We calculated the domain-averaged diurnal cycle of cloud water (Fig. 9) and ice (Fig. 10) mixing ratios for land and ocean grid points separately. Parameterized deep convection (DP) forms thick clouds above the freezing level (Fig. 10a) and weak shallow clouds (Fig. 9a), whereas both EX and SH are able to generate stronger shallow convection as shown by the low-level clouds. Differences in the cloud structure across simulations are likely linked to the mismatch in the timing of precipitation in DP because they are spread over the entire land mass producing rainfall since the early hours. Conversely, low-level clouds in the other two experiments restrain cloud formation in the upper levels and contribute to delay the onset of deep convection with respect to DP , which results in better agreement with the observed diurnal cycle of precipitation.

Accepted for publication in *Journal of Climate*. DOI 10.1175/JCLI-D-19-0416.1.

549 Shallow convection is generally assumed not to produce precipitation (Stensrud 2009). This is
550 true for the shallow convection scheme used, as well as for the BMJ scheme, which also has a
551 shallow convection component. However, it is not necessarily the case for the fully explicit
552 experiment, which may produce some rainfall from shallow convection, thus explaining some of
553 the differences between SH and EX in the diurnal cycle of precipitation. Since both SH and EX
554 are active in the generation of shallow convection as evidenced by the presence of shallow clouds,
555 this could be a reason why they better represent the phase of the precipitation diurnal cycle.
556 Although the timing of the diurnal cycle is corrected by explicitly resolving deep convection, its
557 amplitude, and particularly its peak in the late afternoon (17LST), are too intense compared to the
558 observations. This is partly corrected by the shallow convection scheme, but at the cost of
559 introducing errors over the ocean.
560 We showed that SH produce rainfall rates well below the observational range (circa 50% less
561 on average and up to 90% at some locations) (Fig. 3b), while the other two experiments show a
562 better agreement with observations over the ocean, especially DP. According to the diurnal cycle
563 of the vertical cloud structure (Fig 9 and Fig 10), both simulations explicitly resolving deep
564 convection produce less mid and high clouds than DP, particularly above 7 km, which is likely
565 related to the dry bias over water. Although this feature is also present in EX, it is not as
566 pronounced as in SH. Also, it seems to be compensated to some extent by the formation of low-
567 level clouds that are more intense in EX and are also able to produce some precipitation as opposed
568 to SH.
569 The results above also highlight the importance of the interaction between convection
570 (including explicit convection) and the microphysics scheme, which leads to substantial
571 differences in the vertical structure of clouds and thus rainfall characteristics. Therefore,

Accepted for publication in *Journal of Climate*. DOI 10.1175/JCLI-D-19-0416.1.

differences in precipitation features across convective representations are not only due to different vertical mixing and transport of heat and moisture, but also to a distinct interaction between microphysics and the deep convection scheme. Tests using a different microphysics scheme (Thompson) did not prove superior in terms of precipitation and showed a similar cloud structure (not shown).

4 Summary and discussion

In this study, we quantified the effects of resolution and convective representation in simulating rainfall features and the vertical structure of the atmosphere in the Maritime Continent. In general, increasing resolution and explicitly resolving convection brings both benefits and drawbacks. The timing of the diurnal cycle of precipitation is better captured at convection-permitting scales and with explicit deep convection, but the model produces too much rainfall and exaggerates the amplitude of the diurnal cycle over land. Conversely, switching off the deep convection scheme has a drying effect over the ocean, which emphasized the importance of triggering factors in the explicit convection experiments as opposed to the parameterized ones. This behavior over land and ocean is consistent with previous findings using a range of models and resolutions (e.g. Birch et al., 2015).

We found a positive effect of high resolution in reducing the model precipitation sensitivity to complex orography, as opposed to previous studies (Hassim et al. 2016). Indeed, the wet bias over high-elevated land is alleviated with increased resolution, albeit remaining large even at 2 km. The question of whether this may be solved at even higher resolution remains open, and according to our model results, we can only speculate that grid spaces well below the km scale would be required for that purpose. From a domain-wide perspective, higher resolution leads to generally less precipitation over the ocean and more precipitation over land, although not for all experiments

Accepted for publication in *Journal of Climate*. DOI 10.1175/JCLI-D-19-0416.1.

595 and at all scales. However, wet biases over land are progressively confined to smaller areas and
596 the average mean absolute error is reduced. Results on the diurnal cycle suggest that this
597 improvement comes from better representation of the night and morning rain, while the early
598 evening peak becomes too strong in high resolution runs.

599 Although improving the precipitation diurnal cycle is an indicator of increased realism in the
600 processes producing rainfall, we should not neglect aspects such as the dry bias over the ocean and
601 the exaggerated diurnal peak over land. We have proposed possible mechanisms, which may be
602 interconnected, that explain differences between simulations. For example, using explicit deep
603 convection leads to higher convective available potential energy, which usually indicates a
604 favorable environment for deep convection. However, when the convective parameterization
605 scheme is not used, the model does not trigger convection as readily and is not as efficient as DP
606 in transforming CAPE into deep convective circulation, thus precipitation. Instead, explicit deep
607 convection experiments match the onset of observed precipitation better than the parameterized
608 case because of the marked differences in the cloud structure, which is characterized by widespread
609 deep clouds in the DP simulations as opposed to a shallow layer of clouds generated in both EX
610 and SH. The latter is however slightly different than the fully explicit case because even if they
611 both hold back convection due to their reliance on triggering mechanisms to make the convective
612 potential effective, the shallow convection scheme does not allow for as much accumulation of
613 CAPE as in EX. Also, in the parameterized shallow convection case, the convective inhibition is
614 also slightly larger, which further contributes to hinder convective initiation

615 In view of our results, it is hard to argue that the benefits of increasing resolution over the MC
616 to convection-permitting scales (<4 km) is worth the computational cost. Perhaps, improved
617 realism of precipitation arises when increasing resolution to the kilometre scale or higher, because

Accepted for publication in *Journal of Climate*. DOI 10.1175/JCLI-D-19-0416.1.

the representation of localized convective circulation will be more accurate. In fact, previous studies (Bryan et al. 2003, Caine et al. 2013) argued that at resolutions explored here, models do not resolve entrainment and overturning, and thus tend to exaggerate deep moist convection and produce too much rainfall, which is in agreement with our results. Unfortunately, the evidence gathered in this study does not allow to affirm that even higher resolutions will bring significant improvements and further research is needed in this direction.

Once the convection scheme is turned off and most convective processes are explicitly resolved, the model relies on the microphysics to generate rainfall and on the Planetary Boundary Layer scheme to create the low-level instability required for convection initiation. Our results suggest that these schemes and their interplay are likely to play a non-negligible role in simulating precipitation in the MC with convection-permitting models. However, our study does not delve into the potential impact of factors other than the resolution and the representation of convection. Investigating the effect of microphysics and PBL schemes would add to the results presented here.

The role of evapotranspiration and, to a lesser extent the mesoscale air-sea interactions, have been largely ignored in the context of improving rainfall characteristics over the MC. Our ability to correctly represent them in our modelling efforts seems important so that the right amount of moisture available for convection is provided. These two aspects are interesting directions to continue identifying the dominant factors that may help simulate realistic tropical convective precipitation.

Accepted for publication in *Journal of Climate*. DOI 10.1175/JCLI-D-19-0416.1.

Acknowledgements

This work was supported by the REHIPRE project. REHIPRE is funded by the European Union's Horizon 2020 research and innovation programme under the Marie Skłodowska-Curie Actions Individual Fellowship grant agreement No 743547. This study was also supported by the COASTEPS project (CGL2017-82868-R MEIC/AEI/EU FEDER) financed by the Spanish Ministry of Economy, Industry and Competitiveness, and partially funded by EU FEDER funds. We thankfully acknowledge the computer resources at MareNostrum4 and the technical support provided by the Barcelona Supercomputing Center (RES-AECT-2018-1-0001, RES-AECT-2018-2-0002). We also thank NCAR and other participating institutions for making WRF-ARW model available. As Associate Investigator of the ARC Centre of Excellence for Climate Extremes (Australia), D. Argüeso would also like to thank their scientific and technical support. The authors also thank two anonymous reviewers whose comments significantly improved the paper.

References

Argüeso, D., A. Di Luca, and J. P. Evans, 2016: Precipitation over urban areas in the western Maritime Continent using a convection-permitting model. *Clim. Dyn*, **47**, 1143–1159, https://doi.org/10.1007/s00382-015-2893-6.

Baranowski, D. B., D. E. Waliser, X. Jiang, J. A. Ridout, and M. K. Flatau, 2019: Contemporary GCM Fidelity in Representing the Diurnal Cycle of Precipitation Over the Maritime Continent. *Journal of Geophysical Research: Atmospheres*, **124**, 747–769, https://doi.org/10.1029/2018JD029474.

Betts, A. K., 1986: A new convective adjustment scheme. Part I: Observational and theoretical basis. *Q.J.R. Meteorol. Soc*, **112**, 677–691, https://doi.org/10.1002/qj.49711247307.

Betts, A. K., and M. J. Miller, 1986: A new convective adjustment scheme. Part II: Single column tests using GATE wave, BOMEX, ATEX and arctic air- mass data sets. *Q.J.R. Meteorol. Soc*, **112**, 693–709, https://doi.org/10.1002/qj.49711247308.

Accepted for publication in *Journal of Climate*. DOI 10.1175/JCLI-D-19-0416.1.

668 Bharti, V., C. S. J. O. G. Research, 2015: Evaluation of error in TRMM 3B42V7 precipitation
669 estimates over the Himalayan region. *J. Geophys. Res. Atmos*, **120**, 12458–12473,
670 https://doi.org/10.1002/2015JD023779.

671 Bhatt, B. C., S. Sobolowski, A. Higuchi, 2016: Simulation of diurnal rainfall variability over the
672 Maritime Continent with a high-resolution regional climate model. *Journal of the*
673 *Meteorological Society of Japan*, **94A**, 89–103, https://doi.org/10.2151/jmsj.2015-052.

674 Birch, C. E., M. J. Roberts, L. Garcia-Carreras, D. Ackerley, M. J. Reeder, A. P. Lock, and R.
675 Schiemann, 2015: Sea-Breeze Dynamics and Convection Initiation: The Influence of
676 Convective Parameterization in Weather and Climate Model Biases. *J. Climate*, **28**, 8093–
677 8108, https://doi.org/10.1175/JCLI-D-14-00850.1.

678 Birch, C. E., S. Webster, S. C. Peatman, D. J. Parker, A. J. Matthews, Y. Li, and M. E. E.
679 Hassim, 2016: Scale Interactions between the MJO and the Western Maritime Continent. *J.*
680 *Climate*, **29**, 2471–2492, https://doi.org/10.1175/JCLI-D-15-0557.1.

681 Bryan, G. H., J. C. Wyngaard, and J. M. Fritsch, 2003. Resolution requirements for the
682 simulation of deep moist convection. *Mon. Wea. Rev.*, **131**(10), 2394–2416.
683 http://doi.org/10.1175/1520-0493(2003)131<2394:RRFTSO>2.0.CO;2

684 Caine S., T.P. Lane, P.T. May, C. Jakob, S.T. Siems, M.J. Manton, and J. Pinto, 2013. Statistical
685 Assessment of Tropical Convection-Permitting Model Simulations Using a Cell-Tracking
686 Algorithm, *Mon. Wea. Rev*. **141**, 557–581. doi:10.1175/MWR-D-11-00274.1.

687 Chen, Y., E. E. Ebert, K. J. E. Walsh, and N. E. Davidson, 2013: Evaluation of TRMM 3B42
688 precipitation estimates of tropical cyclone rainfall using PACRAIN data. *J. Geophys. Res.*
689 *Atmos*, **118**, 2184–2196, https://doi.org/10.1002/jgrd.50250.

690 Copernicus Climate Change Service (C3S), 2017: ERA5: Fifth generation of ECMWF
691 atmospheric reanalyses of the global climate. Copernicus Climate Change Service Climate
692 Data Store (CDS), *March 2018*. https://cds.climate.copernicus.eu/cdsapp#!/home

693 Di Luca, A., D. Argüeso, J. P. Evans, R. de Elía, and R. Laprise, 2016: Quantifying the overall
694 added value of dynamical downscaling and the contribution from different spatial scales. *J.*
695 *Geophys. Res. Atmos*, **121**, 1575–1590, https://doi.org/10.1002/2015JD024009.

696 Ebert, E. E., J. E. Janowiak, and C. Kidd, 2007: Comparison of Near-Real-Time Precipitation
697 Estimates from Satellite Observations and Numerical Models. *Bull. Amer. Meteor. Soc*, **88**,
698 47–64, https://doi.org/10.1175/BAMS-88-1-47.

699 Evans, J. P., K. Bormann, J. Katzfey, S. Dean, and R. Arritt, 2016: Regional climate model
700 projections of the South Pacific Convergence Zone. *Clim. Dyn*, **47**, 817–829,
701 https://doi.org/10.1007/s00382-015-2873-x.

702 Gianotti, R. L., D. Zhang, and E. A. B. Eltahir, 2012: Assessment of the Regional Climate Model
703 Version 3 over the Maritime Continent Using Different Cumulus Parameterization and Land
704 Surface Schemes. *J. Climate*, **25**, 638–656, https://doi.org/10.1175/JCLI-D-11-00025.1.

Accepted for publication in *Journal of Climate*. DOI 10.1175/JCLI-D-19-0416.1.

705 Grabowski, W. W., and Coauthors, 2006: Daytime convective development over land: A model
706 intercomparison based on LBA observations. *Q.J.R. Meteorol. Soc*, **132**, 317–344,
707 https://doi.org/10.1256/qj.04.147.

708 Hassim, M. E. E., T. P. Lane, and W. W. Grabowski, 2016: The diurnal cycle of rainfall over
709 New Guinea in convection-permitting WRF simulations. *Atmos. Chem. Phys*, **16**, 161–175,
710 https://doi.org/10.5194/acp-16-161-2016.

711 Hendon, H. H., 2003: Indonesian rainfall variability: Impacts of ENSO and local air-sea
712 interaction. *J. Climate*, **16**, 1775–1790, https://doi.org/10.1175/1520-
713 0442(2003)016<1775:IRVIOE>2.0.CO;2.

714 Hirpa, F. A., M. Gebremichael, and T. Hopson, 2010: Evaluation of High-Resolution Satellite
715 Precipitation Products over Very Complex Terrain in Ethiopia. *J. Appl. Meteor. Climatol*,
716 **49**, 1044–1051, https://doi.org/10.1175/2009JAMC2298.1.

717 Hohenegger, C., P. Brockhaus, and C. Schär, 2008: Towards climate simulations at cloud-
718 resolving scales. *Meteorologische Zeitschrift*, **17**, 383–394, https://doi.org/10.1127/0941-
719 2948/2008/0303.

720 Holloway, C. E., S. J. Woolnough, and G. M. S. Lister, 2012: Precipitation distributions for
721 explicit versus parametrized convection in a large-domain high-resolution tropical case
722 study. *Q.J.R. Meteorol. Soc*, **138**, 1692–1708, https://doi.org/10.1002/qj.1903.

723 Hong, S. Y., and J. Lim, 2006. The WRF single-moment 6-class microphysics scheme (WSM6).
724 *J. Korean Meteor. Soc.*, **42**(2), 129–151.

725 Hong, S.-Y., and J. Jang, 2018: Impacts of Shallow Convection Processes on a Simulated Boreal
726 Summer Climatology in a Global Atmospheric Model. *Asia-Pacific J Atmos Sci*, **54**, 361–
727 370, https://doi.org/10.1007/s13143-018-0013-3.

728 Huffman, G. J., and Coauthors, 2007: The TRMM Multisatellite Precipitation Analysis (TMPA):
729 Quasi-Global, Multiyear, Combined-Sensor Precipitation Estimates at Fine Scales. *J.*
730 *Hydrometeor*, **8**, 38–55, https://doi.org/10.1175/JHM560.1.

731 Huffman, G.J. (2017), GPM IMERG Final Precipitation L3 Half Hourly 0.1 degree x 0.1 degree
732 V05, Greenbelt, MD, Goddard Earth Sciences Data and Information Services Center (GES
733 DISC), Accessed: November 2018, 10.5067/GPM/IMERG/3B-HH/05

734 Im, E. S., and E. Elthair, 2018: Simulation of the diurnal variation of rainfall over the western
735 Maritime Continent using a regional climate model. *Clim. Dyn*,
736 https://doi.org/10.1007/s00382-017-3907-3.

737 Janjic, Z. I., 1994: The step-mountain eta coordinate model: further developments of the
738 convection, viscous sublayer, and turbulence closure schemes. *Mon. Wea. Rev*, **122**, 927–
739 945, https://doi.org/10.1175/1520-0493(1994)122<0927:TSMECM>2.0.CO;2.

Accepted for publication in *Journal of Climate*. DOI 10.1175/JCLI-D-19-0416.1.

740 Joyce, R. J., J. E. Janowiak, and P. A. Arkin, 2004: CMORPH: A method that produces global
741 precipitation estimates from passive microwave and infrared data at high spatial and
742 temporal resolution. *J. Hydrometeor*, **5**, 487–503, https://doi.org/10.1175/1525-
743 7541(2004)005<0487:CAMTPG>2.0.CO;2.

744 Khairoutdinov, M. and D. Randall, 2006: High-resolution simulation of shallow-to-deep
745 convection transition over land. *Journal of the Atmospheric Sciences*, **63**(12), 3421–3436.
746 http://doi.org/10.1175/JAS3810.1

747 Kwan, M. S., F. T. Tangang, and L. Juneng, 2013: Present-day regional climate simulation over
748 Malaysia and western Maritime Continent region using PRECIS forced with ERA40
749 reanalysis. *Theor Appl Climatol*, **115**, 1–14, https://doi.org/10.1007/s00704-013-0873-5.

750 Ladwig, W., 2017. wrf-python (Version 1.3.1) [Software]. Boulder, Colorado: UCAR/NCAR.
751 https://doi.org/10.5065/D6W094P1

752 Lee, M. I., I.S. Kang and B.E. Mapes, 2003: Impacts of cumulus convection parameterization on
753 aqua-planet AGCM simulations of tropical intraseasonal variability. *Journal of the*
754 *Meteorological Society of Japan*, **81**(5), 963–992. http://doi.org/10.2151/jmsj.81.963

755 Leutwyler, D., D. Lüthi, N. Ban, O. Fuhrer, and C. Schär, 2017: Evaluation of the convection-
756 resolving climate modeling approach on continental scales. *J. Geophys. Res. Atmos*, **122**,
757 5237–5258, https://doi.org/10.1002/2016JD026013.

758 Li, Y., N. C. Jourdain, A. S. Taschetto, A. Sen Gupta, D. Argüeso, S. Masson, and W. Cai, 2016:
759 Resolution dependence of the simulated precipitation and diurnal cycle over the Maritime
760 Continent. *Clim. Dyn*, 1–20, https://doi.org/10.1007/s00382-016-3317-y.

761 Love, B. S., A. J. Matthews, and G. M. S. Lister, 2011: The diurnal cycle of precipitation over
762 the Maritime Continent in a high-resolution atmospheric model. *Q.J.R. Meteorol. Soc*, **137**,
763 934–947, https://doi.org/10.1002/qj.809.

764 Matthews, A. J., G. Pickup, S. C. Peatman, P. Clews, and J. Martin, 2013: The effect of the
765 Madden-Julian Oscillation on station rainfall and river level in the Fly River system, Papua
766 New Guinea. *J. Geophys. Res. Atmos*, **118**, 10, 926–10, 935,
767 https://doi.org/10.1002/jgrd.50865.

768 National Center for Atmospheric Research, 2017. *Advanced Research WRF 3.9 User Guide*.
769 Retrieved from http://www2.mmm.ucar.edu/wrf/users/docs/user_guide_V3/contents.html

770 Neale, R., and J. Slingo, 2003: The maritime continent and its role in the global climate: A GCM
771 study. *J. Climate*, **16**, 834–848, https://doi.org/10.1175/1520-
772 0442(2003)016<0834:TMCAIR>2.0.CO;2.

773 Peatman, S. C., A. J. Matthews, and D. P. Stevens, 2013: Propagation of the Madden-Julian
774 Oscillation through the Maritime Continent and scale interaction with the diurnal cycle of
775 precipitation. *Q.J.R. Meteorol. Soc*, **140**, 814–825, https://doi.org/10.1002/qj.2161.

Accepted for publication in *Journal of Climate*. DOI 10.1175/JCLI-D-19-0416.1.

776 Pilon, R., C. Zhang and J. Dudhia 2016: Roles of deep and shallow convection and microphysics
777 in the MJO simulated by the model for prediction across scales. *Journal of Geophysical*
778 *Research*, **121**(18), 10575–10600. http://doi.org/10.1002/2015JD024697

779 Prein, A. F., and Coauthors, 2015: A review on regional convection- permitting climate
780 modeling: demonstrations, prospects, and challenges. *Rev Geophys*, **53**,
781 https://doi.org/10.1002/(ISSN)1944-9208.

782 Qian, J.-H., 2008: Why Precipitation Is Mostly Concentrated over Islands in the Maritime
783 Continent. *J. Atmos. Sci*, **65**, 1428–1441, https://doi.org/10.1175/2007JAS2422.1.

784 Qian, J.-H., A. W. Robertson, and V. Moron, 2010: Interactions among ENSO, the Monsoon,
785 and Diurnal Cycle in Rainfall Variability over Java, Indonesia. *J. Atmos. Sci*, **67**, 3509–3524,
786 https://doi.org/10.1175/2010JAS3348.1.

787 Rahmawati, N., and M. W. Lubczynski, 2017: Validation of satellite daily rainfall estimates in
788 complex terrain of Bali Island, Indonesia. 1–20, https://doi.org/10.1007/s00704-017-2290-7.

789 Rauniyar, S. P., A. Protat, and H. Kanamori, 2017: Uncertainties in TRMM-Era multisatellite-
790 based tropical rainfall estimates over the Maritime Continent. *Earth and Space Science*, **4**,
791 275–302, https://doi.org/10.1002/2017EA000279.

792 Sabin, T.P., C.A. Babu and P.V. Joseph, 2013: SST-convection relation over tropical oceans.
793 *International Journal of Climatology*, **33**, 1424-1435, https://doi.org/10.1002/joc.3522.

794 Schiemann, R., M. E. Demory, M. S. Mizielinski, M. J. Roberts, L. C. Shaffrey, J. Strachan, and
795 P. L. Vidale, 2013: The sensitivity of the tropical circulation and Maritime Continent
796 precipitation to climate model resolution. *Clim. Dyn*, **42**, 2455–2468,
797 https://doi.org/10.1007/s00382-013-1997-0.

798 Schlemmer, L. and C. Hohenegger , 2014: The Formation of Wider and Deeper Clouds as a
799 Result of Cold-Pool Dynamics. *Journal of the Atmospheric Sciences*, **71**(8), 2842–2858.
800 http://doi.org/10.1175/JAS-D-13-0170.1

801 Shige, S., S. Kida, H. Ashiwake, T. Kubota, and K. Aonashi, 2013: Improvement of TMI Rain
802 Retrievals in Mountainous Areas. *J. Appl. Meteor. Climatol*, **52**, 242–254,
803 https://doi.org/10.1175/JAMC-D-12-074.1.

804 Skok, G., N. Žagar, L. Honzak, R. Žabkar, J. Rakovec, and A. Ceglar, 2016: Precipitation
805 intercomparison of a set of satellite- and raingauge-derived datasets, ERA Interim reanalysis,
806 and a single WRF regional climate simulation over Europe and the North Atlantic. *Theor*
807 *Appl Climatol*, **123**, 217–232, https://doi.org/10.1007/s00704-014-1350-5.

808 Stensrud, D. J., 2009: *Parameterization schemes: Keys to Understanding Numerical Weather*
809 *Prediction Models*. Cambridge University Press, 480 pp.

Accepted for publication in *Journal of Climate*. DOI 10.1175/JCLI-D-19-0416.1.

Tan, H., P. Ray, B. S. Barrett, M. Tewari, and M. W. Moncrieff, 2018: Role of topography on the MJO in the maritime continent: a numerical case study. *Clim. Dyn*, **40**, 6252–20, https://doi.org/10.1007/s00382-018-4275-3.

Tan, M., A. Ibrahim, Z. Duan, A. Cracknell, and V. Chaplot, 2015: Evaluation of Six High-Resolution Satellite and Ground-Based Precipitation Products over Malaysia. *Remote Sensing*, **7**, 1504–1528, https://doi.org/10.3390/rs70201504.

Thompson, G., P. R. Field, R. M. Rasmussen, and W. D. Hall, 2008: Explicit forecasts of winter precipitation using an improved bulk microphysics scheme. Part II: Implementation of a new snow parameterization. *Mon. Wea. Rev*, **136**, 5095–5115, https://doi.org/10.1175/2008MWR2387.1.

Tropical Rainfall Measuring Mission (TRMM) (2011), TRMM (TMPA) Rainfall Estimate L3 3-hour 0.25 degree x 0.25 degree V7, Greenbelt, MD, Goddard Earth Sciences Data and Information Services Center (GES DISC), Accessed: January 2018. 10.5067/TRMM/TMPA/3H/7

Vernimmen, R. R. E., A. Hooijer, Mamenun, E. Aldrian, and A. I. J. M. van Dijk, 2012: Evaluation and bias correction of satellite rainfall data for drought monitoring in Indonesia. *Hydrol. Earth Syst. Sci*, **16**, 133–146, https://doi.org/10.5194/hess-16-133-2012.

Vincent, C. L., and T. P. Lane, 2016: Evolution of the Diurnal Precipitation Cycle with the Passage of a Madden–Julian Oscillation Event through the Maritime Continent. *Mon. Wea. Rev*, **144**, 1983–2005, https://doi.org/10.1175/MWR-D-15-0326.1.

Vincent, C. L., and T. P. Lane, 2017: A 10-Year Austral Summer Climatology of Observed and Modeled Intraseasonal, Mesoscale, and Diurnal Variations over the Maritime Continent. *J. Climate*, **30**, 3807–3828, https://doi.org/10.1175/JCLI-D-16-0688.1.

Vincent, C. L., and T. P. Lane, 2018: Mesoscale Variation in Diabatic Heating around Sumatra, and Its Modulation with the Madden–Julian Oscillation. *Mon. Wea. Rev*, **146**, 2599–2614, https://doi.org/10.1175/MWR-D-17-0392.1.

Wagner, A., D. Heinzeller, S. Wagner, T. Rummler, and H. Kunstmann, 2018: Explicit Convection and Scale-Aware Cumulus Parameterizations: High-Resolution Simulations over Areas of Different Topography in Germany. *Mon. Wea. Rev*, **146**, 1925–1944, https://doi.org/10.1175/MWR-D-17-0238.1.

Yamanaka, M. D., S.-Y. Ogino, P.-M. Wu, H. Jun-Ichi, S. Mori, J. Matsumoto, and F. Syamsudin, 2018: Maritime continent coastlines controlling Earth's climate. 1–28, https://doi.org/10.1186/s40645-018-0174-9.

Yilmaz, K. K., T. S. Hogue, K. L. Hsu, S. Sorooshian, H. V. Gupta, and T. Wagener, 2005: Intercomparison of rain gauge, radar, and satellite-based precipitation estimates with emphasis on hydrologic forecasting. *J. Hydrometeor*, **6**, 497–517, https://doi.org/10.1175/JHM431.1.

Accepted for publication in *Journal of Climate*. DOI 10.1175/JCLI-D-19-0416.1.

847

848

849

850

851

852

853

854

855

856

Accepted for publication in *Journal of Climate*. DOI 10.1175/JCLI-D-19-0416.1.

857 **Table 1:** Summary of the experiments completed for this study. All experiments refer to the
858 period 1 November 2015 to 29 February 2016

	Parameterized Deep and Shallow Convection	**Parameterized shallow convection and explicit deep convection**	**Fully-explicit convection**
Acronym	**DP**	**SH**	**EX**
Convective parameterization	Betts-Miller-Janjic (cu_physics = 2, shcu_physics = 0)	GRIMS shallow convection (cu_physics = 0, shcu_physics = 3)	No convective parameterization (cu_physics = 0, shcu_physics = 0)
Planetary Boundary Layer Parameterization	Yonsei University scheme (bl_pbl_physics = 1)		
Radiation (Longwave)	Rapid Radiative Transfer Model scheme (ra_lw_physics = 1)		
Radiation (Shortwave)	Goddard shortwave (ra_sw_physics = 2)		
Microphysics	WRF Single-Moment 6-class scheme (mp_physics = 6)		
Land surface	Noah Land Surface scheme (sf_surface_physics = 2)		
Surface layer	MM5 simmilarity scheme (sf_sfclay_physics = 1)		
Vertical coordinate	Hybrid vertical coordinate (hybrid_opt = 2)		
Horizontal difussion	2-D Smagorinsky scheme and implicit mixing in the 6^{th}-order horizontal diffusion filter		
Resolution	32, 16, 8, 4, and 2 km		

859

860

Accepted for publication in *Journal of Climate*. DOI 10.1175/JCLI-D-19-0416.1.

Table 2: Simulations ranked (1 is best, 15 is worst) according to their performance with respect to the observations average in different metrics of the diurnal cycle (amplitude, mean, time of maximum and time of minimum). Actual values are shown in Figure 3. Best and worst performing experiments are highlighted with bold font.

		LAND				**OCEAN**			
Res	**Exp**	**Amplitude**	**Mean**	**Time of Max**	**Time of Min**	**Amplitude**	**Mean**	**Time of Max**	**Time of Min**
32km	**DP**	3	**15**	6	9	10	9	**1**	9
	SH	**1**	**1**	**14**	9	**15**	**15**	10	**1**
	EX	2	2	**14**	**15**	13	10	**13**	**15**
16km	**DP**	4	13	6	9	9	7	**1**	9
	SH	5	4	11	7	14	14	**13**	**1**
	EX	6	6	13	7	7	5	**13**	13
8km	**DP**	7	7	6	9	5	3	**1**	9
	SH	9	9	4	**1**	12	11	10	**1**
	EX	13	10	4	**1**	**1**	4	6	**1**
4km	**DP**	8	5	6	9	4	**1**	**1**	9
	SH	11	8	**1**	**1**	11	12	10	**1**
	EX	**15**	12	**1**	**1**	2	6	6	**1**
2km	**DP**	10	3	12	9	6	2	**1**	14
	SH	12	11	6	**1**	8	13	6	**1**
	EX	14	14	**1**	**1**	3	8	6	**1**

Accepted for publication in *Journal of Climate*. DOI 10.1175/JCLI-D-19-0416.1.

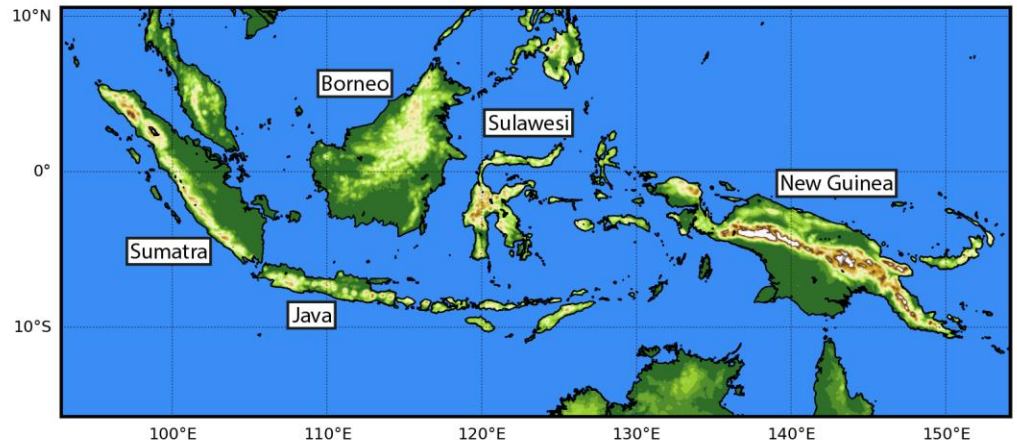

Figure 1: The Maritime Continent. Labels indicate names of major islands. The region shown corresponds exactly to the model domain.

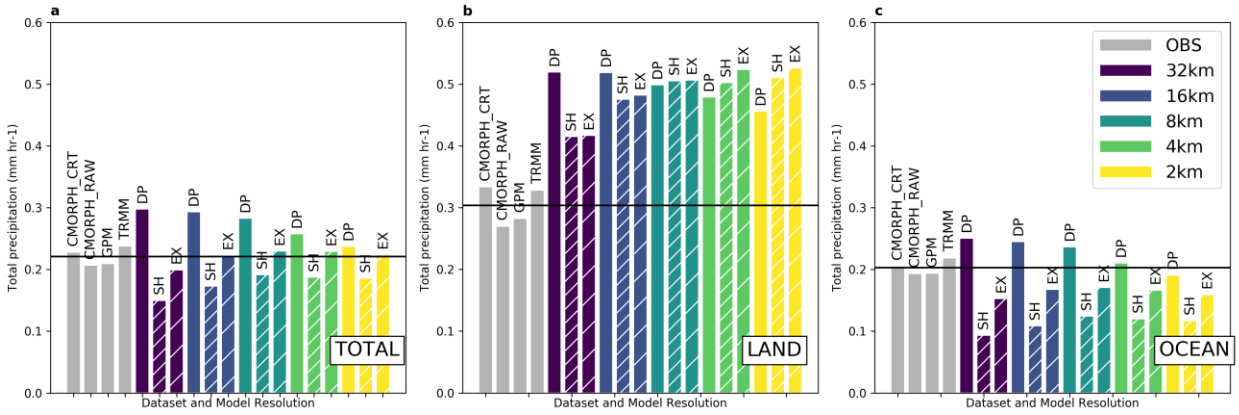

Figure 2: Total precipitation from satellite-derived observations (gray) and different model experiments (colored) over the entire domain (a), land-only grid points (b) and ocean-only grid points (c). The horizontal black line represents the average of the four observational products.

Accepted for publication in *Journal of Climate*. DOI 10.1175/JCLI-D-19-0416.1.

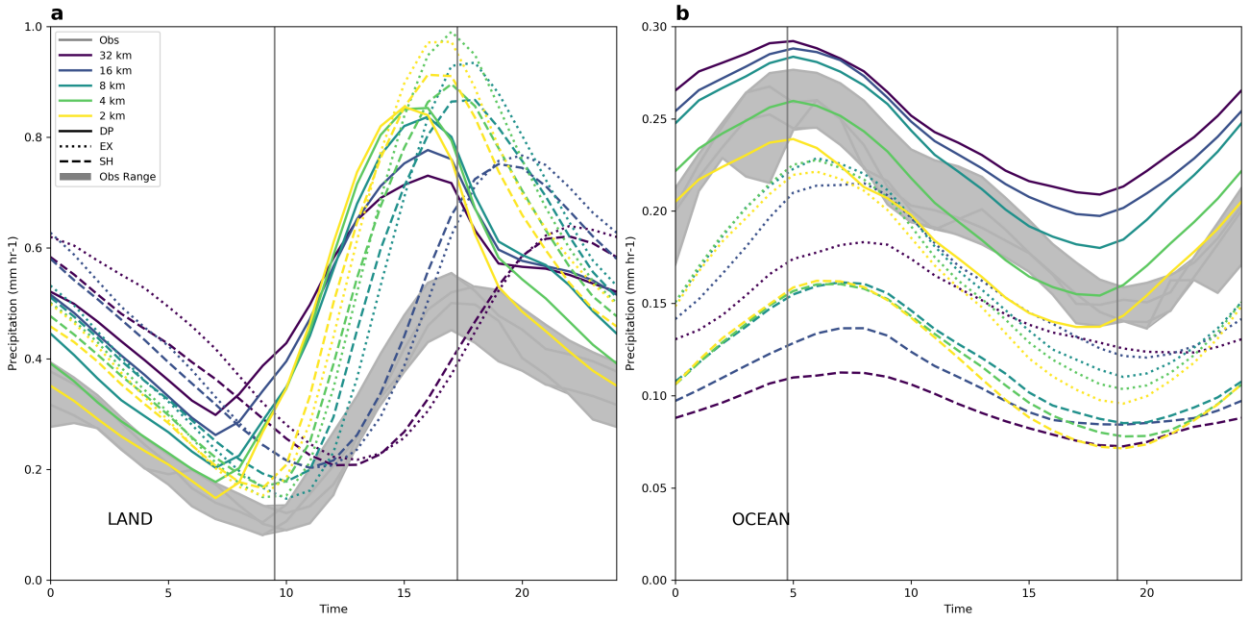

Figure 3: Precipitation diurnal cycle over land (a) and ocean (b) averaged over the entire domain from the satellite-derived observations (gray) and model experiments at different resolutions (colored) with parameterized deep and shallow convection (solid lines), parameterized shallow convection only (dashed line) and fully-explicit convection (dotted lines). Vertical grey lines denote the average time of the minimum and maximum of the precipitation diurnal cycle from all observations.

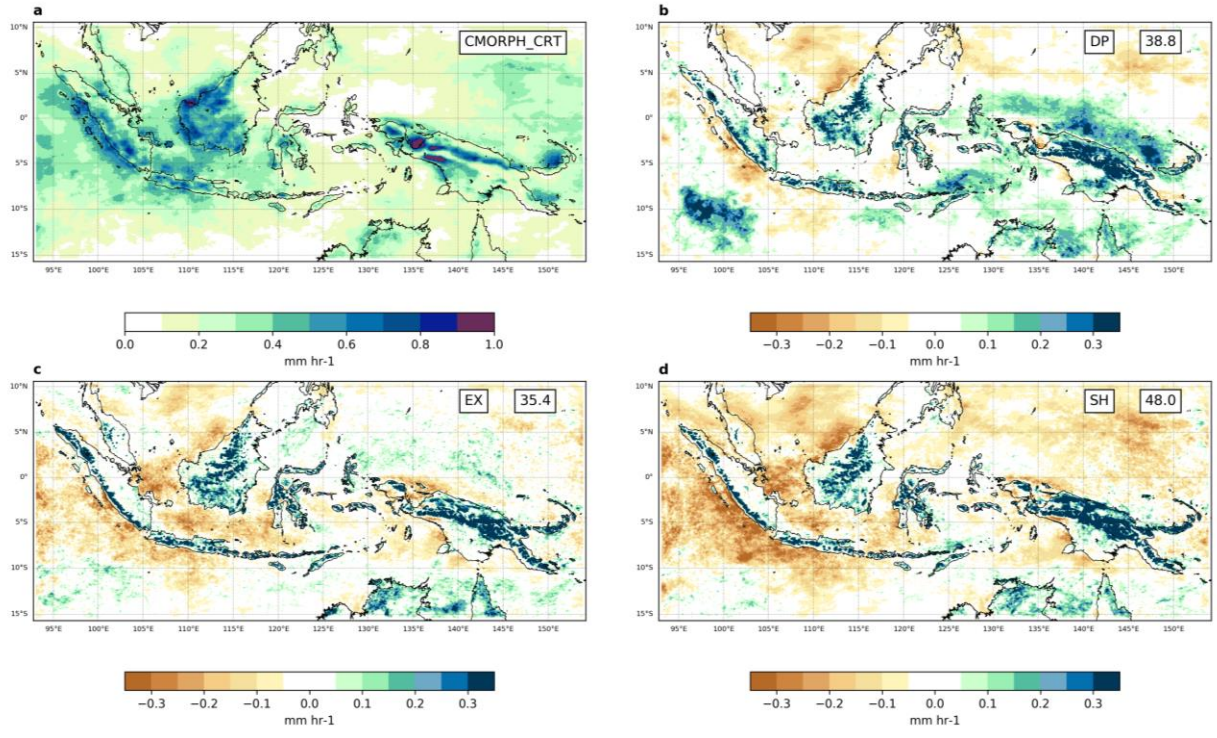

Figure 4: Total precipitation between 1 November 2015 and 29 February 2016 from satellite-derived observations CMORPH_CRT (a) and biases (mm hr-1) between three 4-km model

Accepted for publication in *Journal of Climate*. DOI 10.1175/JCLI-D-19-0416.1.

883 experiments and the range of total precipitation from available observational products. The model
884 experiments differ in their representation of convective processes: Parameterized deep and shallow
885 convection (b), Parameterization of shallow convection only and explicit deep convection (c) and
886 fully-explicit convection (d). The top-right box in each panel plot shows the mean absolute error
887 averaged over the domain in percentage units with respect to observations.

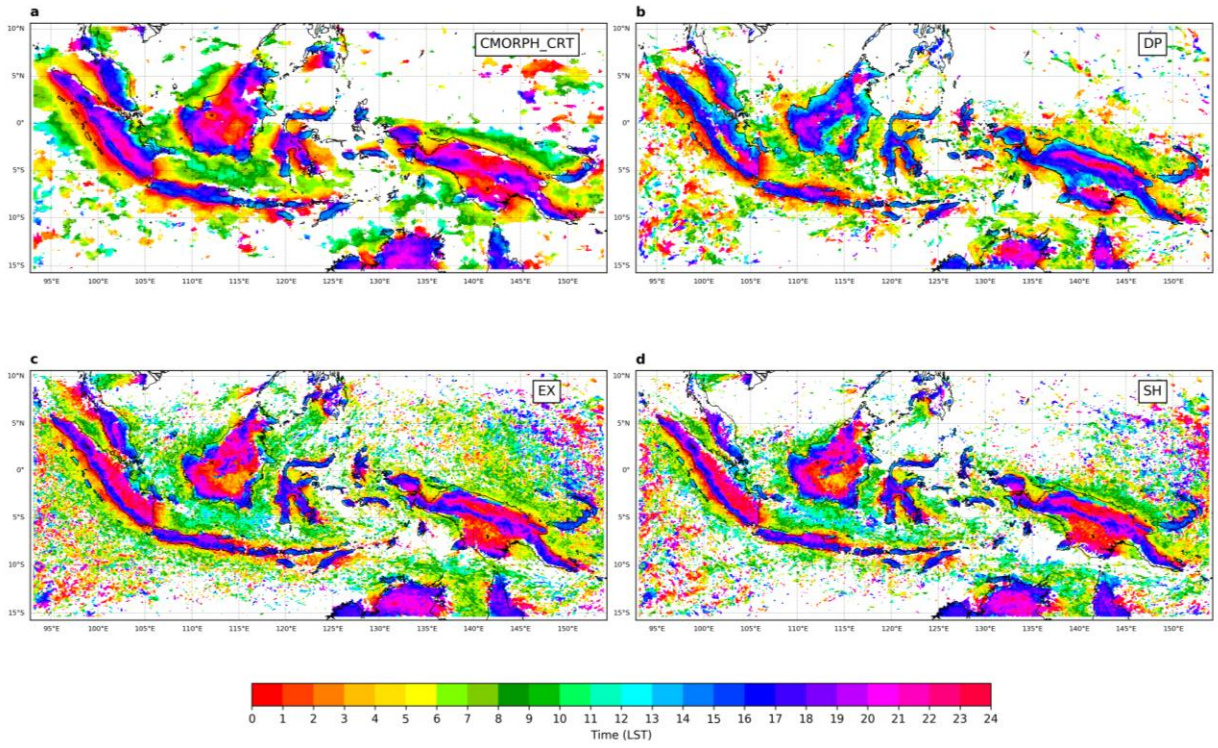

888

889 **Figure 5:** Time of diurnal precipitation maximum calculated from the diurnal cycle fitted to the
890 diurnal harmonic for CMORPH_CRT (a) and three 4-km model simulations: parameterized deep
891 convection (b), parameterized shallow convection only (c) and fully-explicit convection (d). Areas
892 where the amplitude of the cycle is less than 0.1 mm hr^{-1} are masked in white.

Accepted for publication in *Journal of Climate*. DOI 10.1175/JCLI-D-19-0416.1.

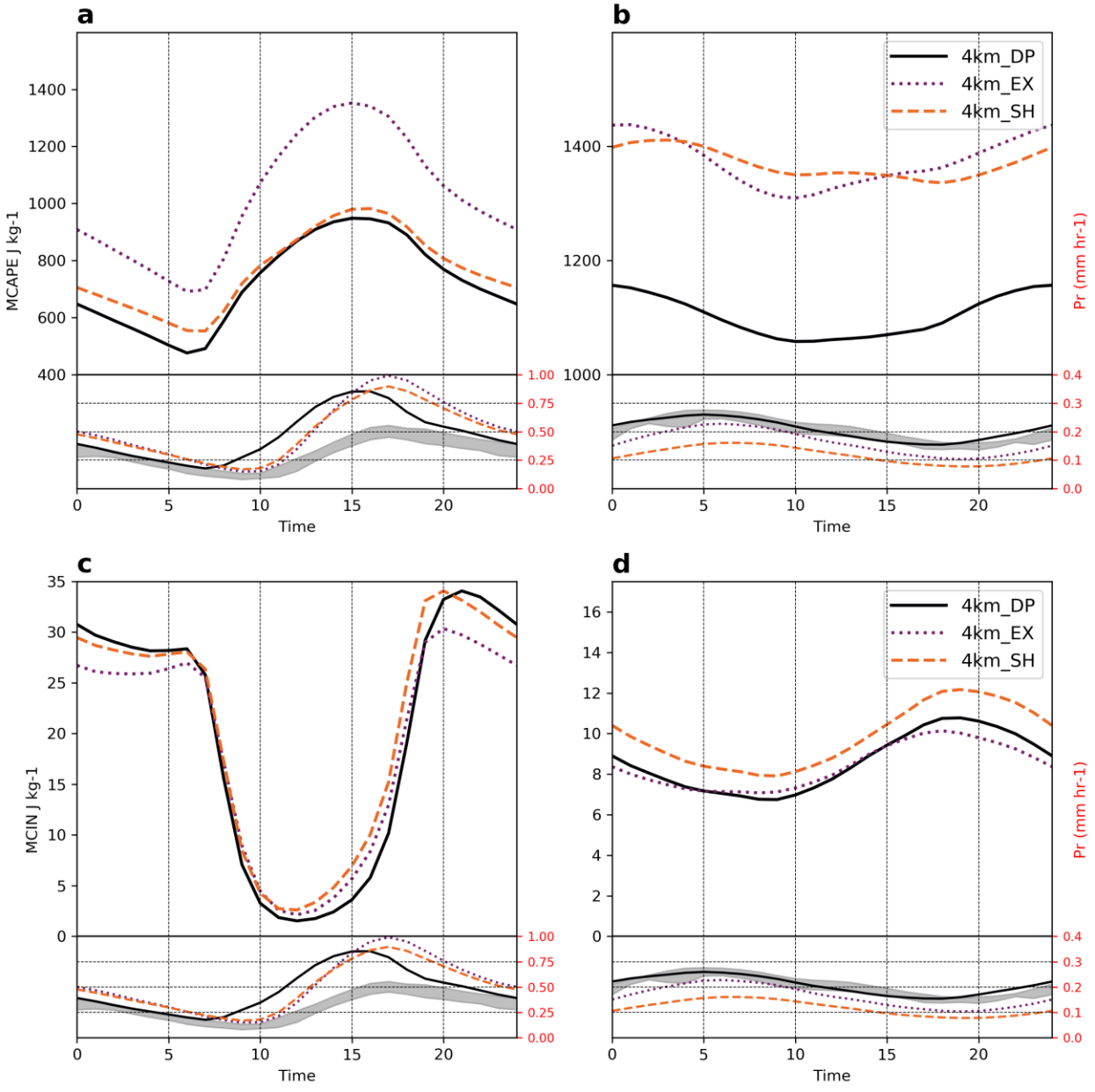

Figure 6: Diurnal evolution of domain-averaged convective available potential energy (CAPE) over land (a) and ocean (b), and convective inhibition (CIN) energy over land (c) and ocean (d). At the bottom of each panel, the diurnal cycle of precipitation is shown for observations (grey range) and all model simulations over land (a, c) and ocean (b, d). Both CAPE and CIN were calculated for the parcel with highest equivalent potential temperature in the lowest 3000 m. Note that scales for land and ocean are different.

Accepted for publication in *Journal of Climate*. DOI 10.1175/JCLI-D-19-0416.1.

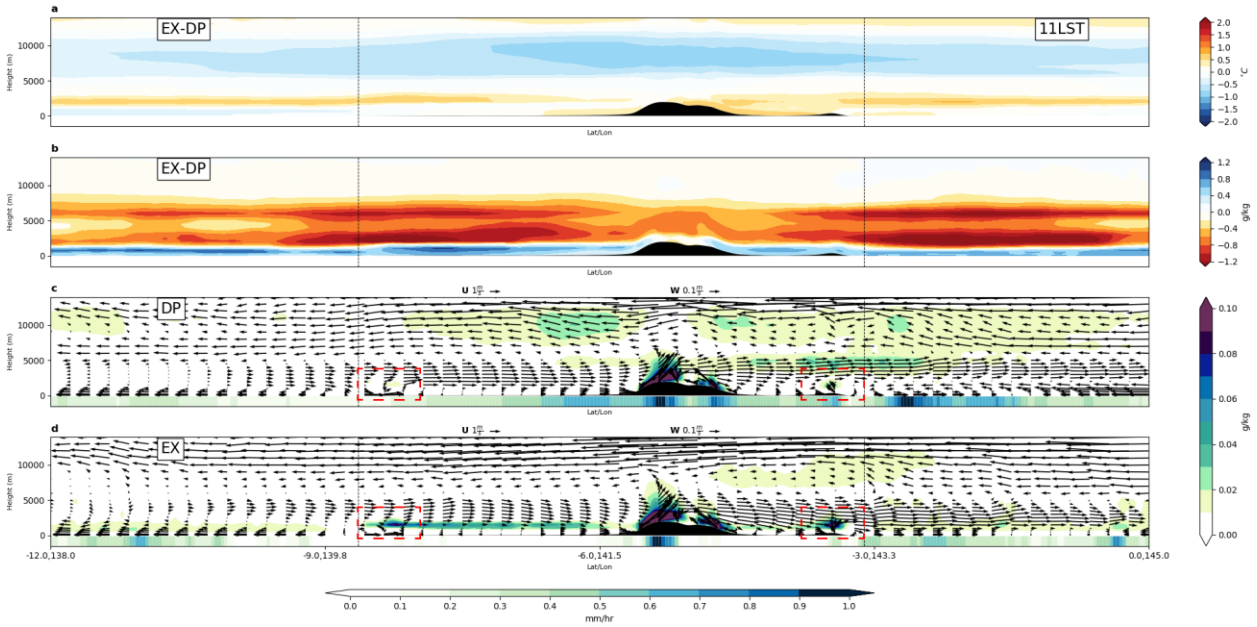

904

905 **Figure 7:** Vertical cross-sections at 11LST across New Guinea of temperature differences between
906 EX and DP (a), mixing ratio differences between EX and DP (b), cloud mixing ratio (water and
907 ice), winds along transect and precipitation (bottom bar) for DP (c) and EX (d). Black shading
908 shows topography and vertical dashed lines indicate the location of coastlines. Dashed red
909 rectangles indicate the location of the sea-breeze front.

910

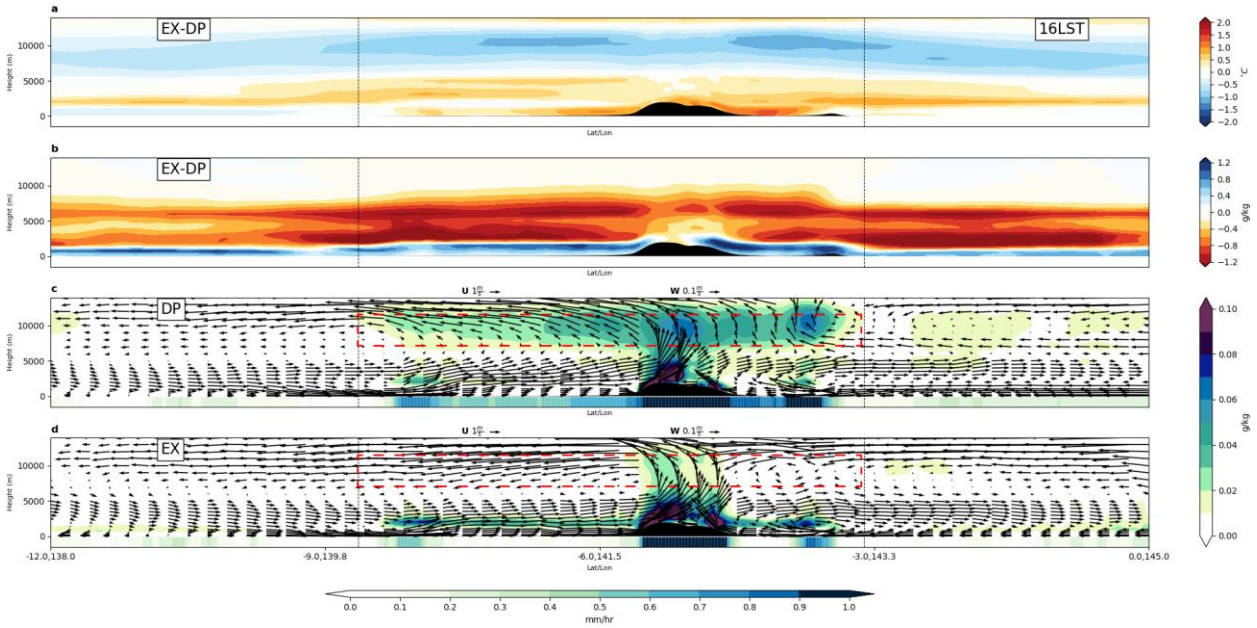

911

912 **Figure 8:** As Figure 7 but at 16LST. Dashed red rectangles highlight wind patterns differences
913 across simulations in the upper troposphere.

914

Accepted for publication in *Journal of Climate*. DOI 10.1175/JCLI-D-19-0416.1.

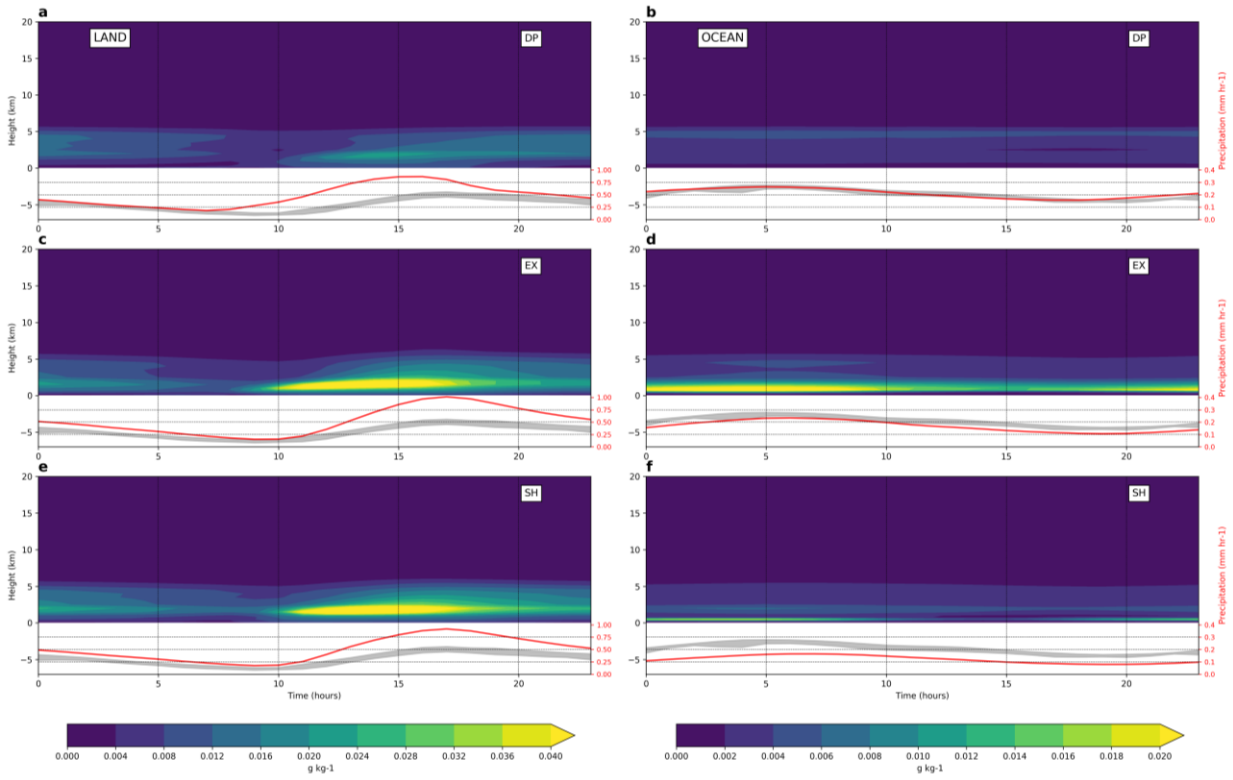

Figure 9: Diurnal evolution of the vertical structure of the cloud water mixing ratio in different simulations at 4 km. The cloud water mixing ratio is represented as a function of height (km) and hour of the day (hours) over land (left column) and ocean (right column) grid points for the entire domain. Parameterized deep convection experiments (EX) are in the first row (a, b), fully explicit convection runs (EX) in the middle row (c, d) and parameterized shallow convection runs (SH) are in the bottom row (e, f). At the bottom of each panel the diurnal cycle of precipitation is shown for the corresponding experiment (red) and the range of observations (grey)

Accepted for publication in *Journal of Climate*. DOI 10.1175/JCLI-D-19-0416.1.

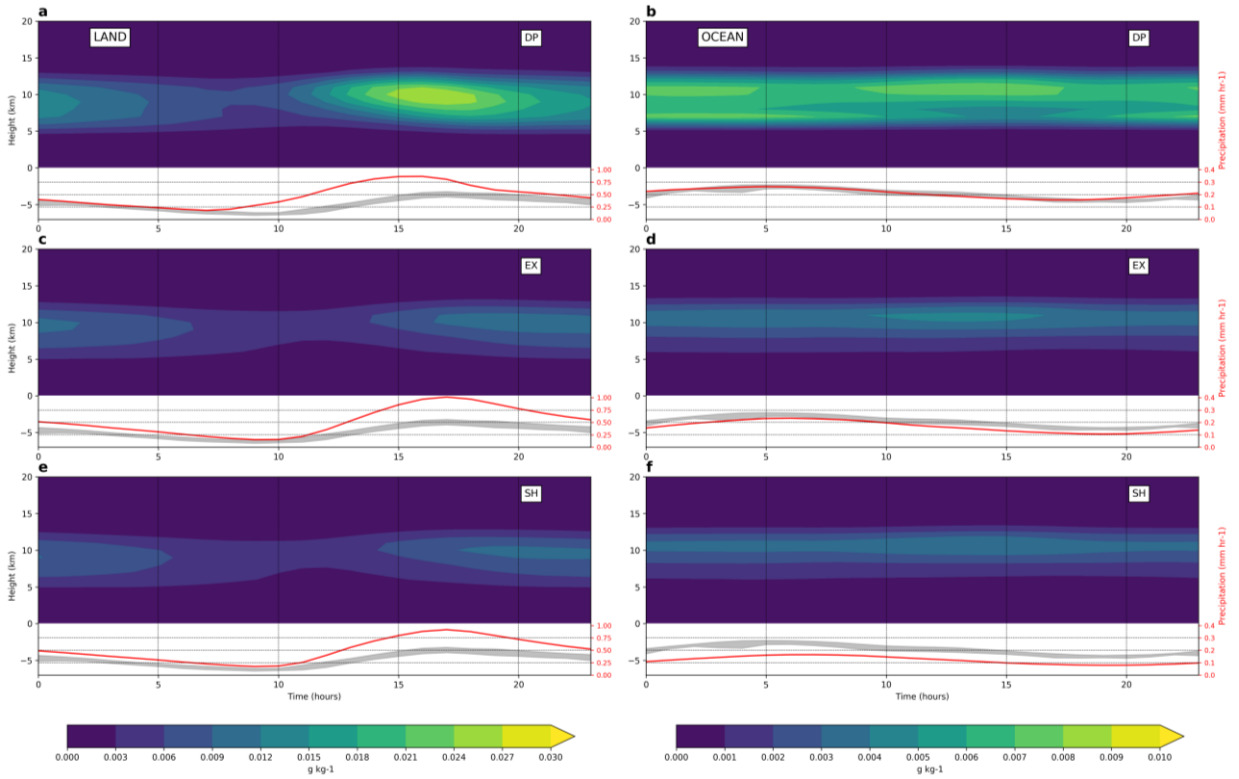

925

926 **Figure 10:** As Figure 9 but for cloud ice mixing ratio.

927

928

929

Accepted for publication in *Journal of Climate*. DOI 10.1175/JCLI-D-19-0416.1.